



Ultrathin pre-lithiated V_6O_{13} nanosheet cathodes with enhanced electrical transport and cyclability



Xiacong Tian^{a,1}, Xu Xu^{a,1}, Liang He^a, Qjulong Wei^a, Mengyu Yan^a, Lin Xu^b, Yunlong Zhao^a, Chuchu Yang^a, Liqiang Mai^{a,*}

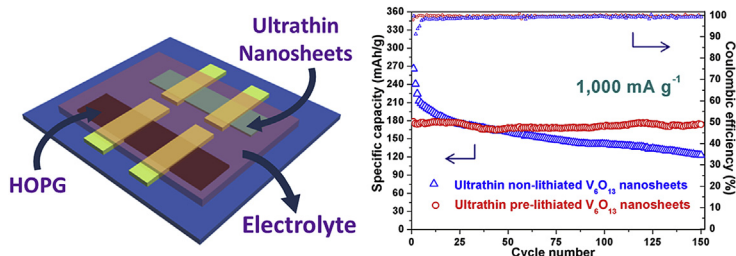
^aState Key Laboratory of Advanced Technology for Materials Synthesis and Processing, WUT-Harvard Joint Nano Key Laboratory, Wuhan University of Technology, Wuhan 430070, China

^bDepartment of Chemistry and Chemical Biology, Harvard University, Cambridge, MA 02138, USA

HIGHLIGHTS

- The ultrathin pre-lithiated V_6O_{13} nanosheets with 4 nm thickness are prepared.
- The smallest electrochemical devices based on nanosheet cathodes are fabricated.
- Intrinsic electrical conductivity change is *in situ* investigated at single nanosheet level.
- The as-synthesized material delivers a high initial discharge capacity of 331 mAh g^{-1} .
- The high capacity retention of 98% is achieved after 150 cycles.

GRAPHICAL ABSTRACT



ARTICLE INFO

Article history:

Received 21 November 2013

Received in revised form

24 December 2013

Accepted 4 January 2014

Available online 10 January 2014

Keywords:

Ultrathin nanosheets

Pre-lithiation

Electrochemical devices

Vanadium oxides

Electrical transport

Lithium batteries

ABSTRACT

The novel ultrathin pre-lithiated V_6O_{13} nanosheets are prepared through a low-temperature exfoliation in argon followed by a secondary hydrothermal lithiation. The smallest electrochemical devices based on nanosheet cathodes are fabricated to *in situ* probe the intrinsic advantages of pre-lithiated nanosheets. Pre-lithiated nanosheets show one order of magnitude higher in electrical conductivity compared with non-lithiated nanosheets. The conductance of ultrathin pre-lithiated V_6O_{13} nanosheets still remains at the same level after discharge process while that of ultrathin non-lithiated nanosheets decreases over two orders of magnitude. The electrochemical performances of nanosheet cathodes before and after pre-lithiation are compared to further demonstrate the enhancement of the pre-lithiation. Ultrathin pre-lithiated V_6O_{13} nanosheet cathodes exhibit a high discharge capacity of 301 mAh g^{-1} at the current density of 100 mA g^{-1} . At a higher current density of 1000 mA g^{-1} , the capacity retention after 150 cycles of ultrathin V_6O_{13} nanosheet cathodes is greatly improved from 46% to 98% after pre-lithiation. The enhanced electrical conductance, excellent discharge capacities and cycling performance demonstrate the great potential of ultrathin pre-lithiated V_6O_{13} nanosheets in next-generation high-performance energy storage applications.

© 2014 Elsevier B.V. All rights reserved.

1. Introduction

Rechargeable lithium batteries with high energy density and long-term stability are considered as one of the most suitable candidates applied for portable electronics [1–3]. However, current

* Corresponding author. Tel.: +86 27 87467595.

E-mail address: mlq518@whut.edu.cn (L. Mai).

¹ These authors contributed equally to this work.

lithium batteries suffer from low discharge capacity during the fast charge and discharge processes. Thus it is important but challenging to develop high-capacity and high-rate batteries [4,5]. As is well known, layered vanadium oxides (e.g., V_2O_5 , V_6O_{13} , and VO_2) are promising cathode materials, owing to their high capacity, moderate voltage, and low cost [6–9]. In these vanadium oxides, V_6O_{13} has been demonstrated as one of the leading candidates due to the combination of high theoretical specific capacity and electronic conductivity [7,10,11]. Theoretically, it can electrochemically accommodate up to eight Li per formula which can create more Li^+ participation during lithium insertion and extraction [12]. Moreover, the metallic character it shows at room temperature makes it possible to undertake high rate charge and discharge [13]. Therefore, it is extremely necessary to obtain V_6O_{13} cathodes with desirable lithium storage performance. Nevertheless, as a mixed-valence vanadium oxide, it faces the challenge of controllable structural synthesis and its high rate electrochemical performance was unexplored [14]. On the other hand, the decrease of specific discharge capacity during charge and discharge process also limits the applications in lithium storage [7,15].

Ultrathin nanosheet electrodes, which can provide short lithium diffusion paths and extremely large surface area, are ideal materials for electrochemical devices [16–19]. Recently a series of ultrathin nanosheets have been extensively reported with high specific capacities, demonstrating the great advantages and prospects of two-dimensional (2D) nanostructures for electrochemical device [20–26]. However, it is worth noting that, during the charge/discharge process, some ultrathin nanosheets suffer from the poor cycling stability due to the decrease of intrinsic electronic conductivity or crystal structural fracture [16,26]. To overcome these limitations, some research has focused on the cation intercalation of nanosheets, for example, $Ti_3C_2T_x$ nanosheets, and obvious electrochemical enhancements have been observed [27,28]. Our previous work has provided the direct relationship between electrical transport and electrochemical properties [29]. Revealing the intrinsic electrical changes is very important. However, confined by the detecting technology, to date, direct evidence, such as *in situ* electrochemical characterization by nanodevices before and after lithiation, have not been provided for nanosheets. Besides, thinner nanosheet cathodes should be applied to better evaluate the influence of intrinsic physical mechanism.

Here, we report a facile approach of novel ultrathin V_6O_{13} nanosheets with an average thickness of 4.0 nm. To increase its electrical transport and electrochemical performance when retaining its crystal structure and ultrathin nanosheet morphology, we used a pre-lithiation strategy in the following step to obtain ultrathin pre-lithiated V_6O_{13} nanosheets. A hydrothermal pre-lithiation method was adopted because it can provide an effective approach to pre-insert lithium into the V_6O_{13} ultrathin nanosheets through a high-pressure hydrothermal process. The great enhancements in electrical conductivity of ultrathin pre-lithiated V_6O_{13} nanosheets were confirmed through *in situ* investigation in the nanosheet cathodes based binder-free electrochemical devices. The ultrathin non-lithiated and lithiated V_6O_{13} nanosheet cathodes were further evaluated in two-electrode coin-type cells. The electrochemical performance of ultrathin nanosheet cathodes is significantly improved as well as the electrical conductivity after lithiation. The desirable discharge capacities are presented during the charge and discharge process, even at the very high current density. Due to the pre-lithiation enhancement, an excellent cycling stability of 98% capacity retention was further realized while that of non-lithiated sample only reached 46%. When the current density turned back from high current density to lower current density, 99.5% of the capacity is recovered for ultrathin pre-lithiated V_6O_{13}

nanosheets, showing an excellent rate performance. These results demonstrate that ultrathin pre-lithiated V_6O_{13} nanosheets have the great potential for next-generation high-performance energy storage applications.

2. Experimental

2.1. Synthesis processes

The ultrathin V_6O_{13} nanosheets were prepared in two steps. First, 0.85 g ammonium metavanadate and 1.06 g oxalic acid dihydrate were dissolved in 30 mL distilled water under vigorous stirring for 1 h and yellow–green solution was obtained. Afterward, the solution was transferred into 50 mL Teflon lined autoclave and kept in an oven at 180 °C for 44 h. Flowerlike $NH_4V_4O_{10}$ nanosheets were finally collected by centrifugation and washed several times with distilled water. After dried at 80 °C overnight, the collected powder was then calcined at 450 °C for 8 h in argon (Fig. S1) and the ultrathin V_6O_{13} nanosheets were obtained. Pre-lithiation enhanced ultrathin V_6O_{13} nanosheets were obtained by the similar method we described previously [30]. 0.20 g V_6O_{13} nanosheets were fully dispersed in deionized water by ultrasonic treatment, followed by stirring with 0.29 g lithium chloride monohydrate for 2 days. Then resultant solution was transferred to a 50 mL Teflon lined autoclave and the autoclave was sealed and kept at 180 °C for 24 h. The final product was washed with deionized water for six times and then dried at 70 °C for 24 h.

2.2. Material characterizations

The X-ray diffraction (XRD) measurements were performed to investigate the crystallographic information using a D8 Advance X-ray diffractometer with $Cu K\alpha$ radiation ($\lambda = 1.5418 \text{ \AA}$) in a 2 range from 10° to 70° at room temperature. Field emission scanning electron microscopic (FESEM) images were collected with a JEOL JSM-7100F microscope at an acceleration voltage of 10 kV. The atomic force microscopic (AFM) observation was achieved using Bruker MultiMode 8 Atomic Force Microscope. Transmission electron microscopic (TEM) images were recorded using a JEOL JEM-2010 FEF microscope.

2.3. Electrochemical device fabrication

HOPG flakes were dry transferred onto a marked substrate and V_6O_{13} nanosheets were deposited onto the region close to the HOPG flakes followed by current collector patterning with e-beam lithography and deposition of Cr/Au (5/50 nm) and SU-8 2002, respectively. Then the commercial electrolyte was dropped cast onto the substrate to cover the V_6O_{13} nanosheets and HOPG flakes.

2.4. Electrical and electrochemical measurements

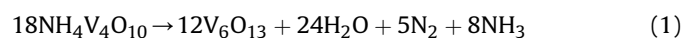
The discharge process of electrochemical devices was performed through cyclic voltammetry and electrical transport properties of electrochemical devices were measured by Agilent B1500A Semiconductor Device Analyzer. The electrochemical properties were tested with 2025 coin cells assembled in a glove box filled with pure argon gas. Lithium pellets were used as the anodes and 1 M solution of $LiPF_6$ in ethylene carbon/dimethyl carbonate was used as the electrolyte. The cathodes were fabricated by mixing 70% V_6O_{13} nanosheets active material, 20% acetylene black and 10% poly(tetrafluoroethylene) and then punched into small disks. Galvanostatic charge/discharge measurement was performed in the potential range from 4.0 to 1.5 V vs Li/Li^+ with a multichannel battery testing system (LAND CT2001A). Cyclic voltammetry was

tested with a CHI 760D electrochemical workstation. Electrochemical impedance spectroscopy (EIS) was tested with an Autolab PGSTAT 302N. All the measurements were carried out at room temperature.

3. Results and discussion

3.1. Structure and morphology

V_6O_{13} nanosheets were obtained in two steps as outlined in Fig. 1g. $NH_4V_4O_{10}$ nanoflowers with ultrathin petal-shaped structure and poor crystallinity (Fig. 1b, S2) were firstly synthesized by a facile hydrothermal method, and then ultrathin V_6O_{13} nanosheets could be achieved from the heat-treatment in argon. The NH_3 decomposed from $NH_4V_4O_{10}$ acted as the reductant. A mixed valence state, +4.33 of vanadium is achieved from the following reaction in the heat-treatment process:



The pre-lithiation method was conducted in the further step to prepare the lithiated V_6O_{13} nanosheets. The crystal structures of as-prepared samples are demonstrated in the XRD pattern (Fig. 1a). For non-lithiated sample, all the diffraction peaks are indexed to the monoclinic V_6O_{13} phase (JCPDS Card No. 89-0100, space group: C2/m) in which single and double vanadium oxide layers alternately stack along the *c*-axis direction in the crystal structure (Fig. S3). No peaks of any other phases are detected, indicating the

high purity of the V_6O_{13} nanosheets. It is confirmed that the main crystalline structure is well remained after lithiation, while a new peak at 20.3° was observed which may be due to a generation of little impurity phase resulting from the lithium ion pre-intercalation process.

According to the representative field emission scanning electron microscopic (FESEM) images (Fig. 1c and e) and transmission electron microscopic (TEM) images (Fig. 1d and f), both products present the nanosheet morphology. After the lithiation process, the nanosheet morphology shows no obvious change. At a higher magnification (Fig. 1d, inset), there are lattice fringes for non-lithiated sample with lattice spacings of 0.35 and 0.27 nm, corresponding to the (110) and (310) planes of V_6O_{13} , respectively. Ultrathin V_6O_{13} nanosheets show the major exposure of (001) facets, along *c*-axis direction. The single-crystal nature of both products was confirmed by selected area electron diffraction (SAED) patterns (Fig. 1d and f, insets).

The tapping mode atomic force microscopy (AFM) was then utilized to measure the thicknesses of the nanosheets before and after the lithiation (Fig. 2). Two average thicknesses of 4.0 and 4.2 nm are shown before and after the lithiation, respectively. This desirable V_6O_{13} ultrathin morphology can be attributed to two reasons during the annealing process. In the first place, the ultrathin petal-shaped nanoflowers scatter into ultrathin nanosheets. Secondly, the escape of NH_3 inside the crystal structure of flower-like $NH_4V_4O_{10}$ nanosheets can lead to an interlayer expansion and a decreased thickness during the heat-treatment procedure. In contrast with non-lithiated sample, the slight distinction in

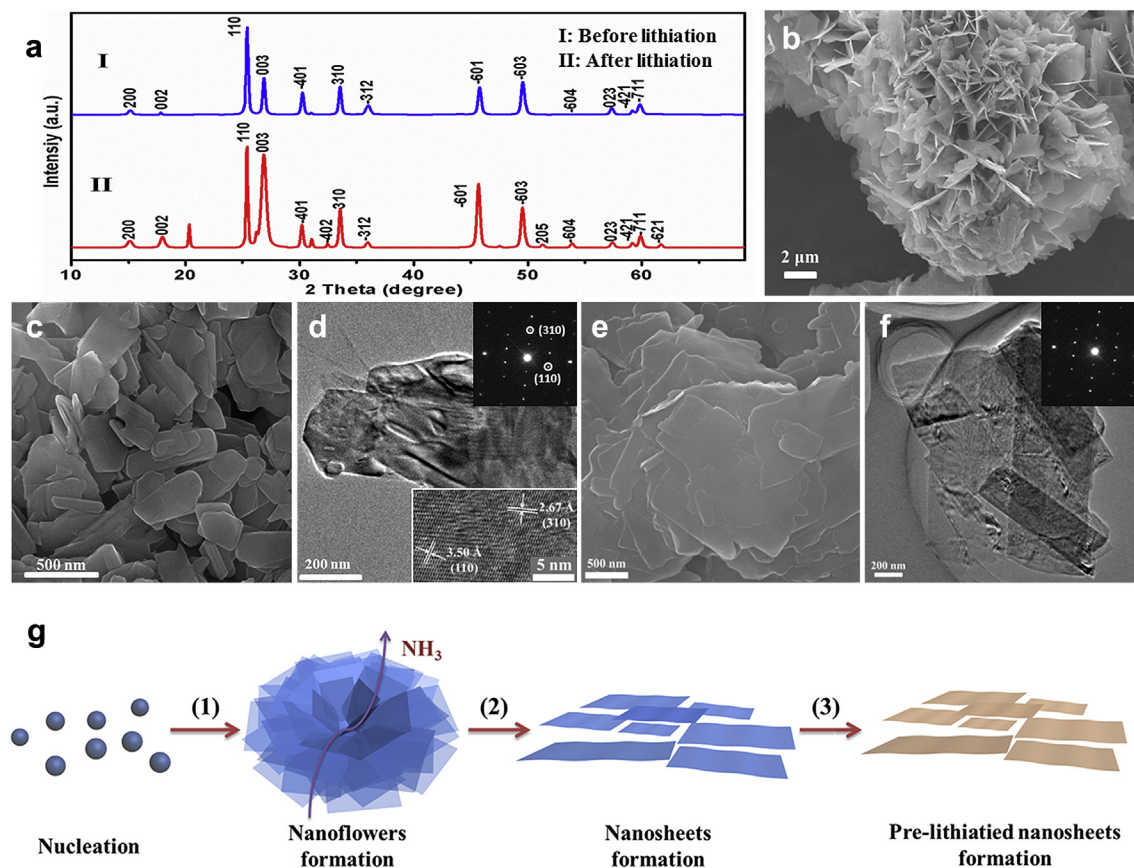


Fig. 1. (a) XRD patterns of as-prepared ultrathin V_6O_{13} nanosheets; SEM images of (b) $NH_4V_4O_{10}$ nanosheets, (c) ultrathin non-lithiated V_6O_{13} nanosheets, and (e) ultrathin lithiated V_6O_{13} nanosheets; TEM images of (d) ultrathin non-lithiated V_6O_{13} nanosheets and (f) ultrathin lithiated V_6O_{13} nanosheets; (g) Schematic illustration of the formation of ultrathin lithiated V_6O_{13} nanosheets. The HRTEM image of ultrathin non-lithiated V_6O_{13} nanosheets is shown in the inset of Fig. 1d (lower). The corresponding SAED patterns are shown in the insets Fig. 1d (upper) and f.

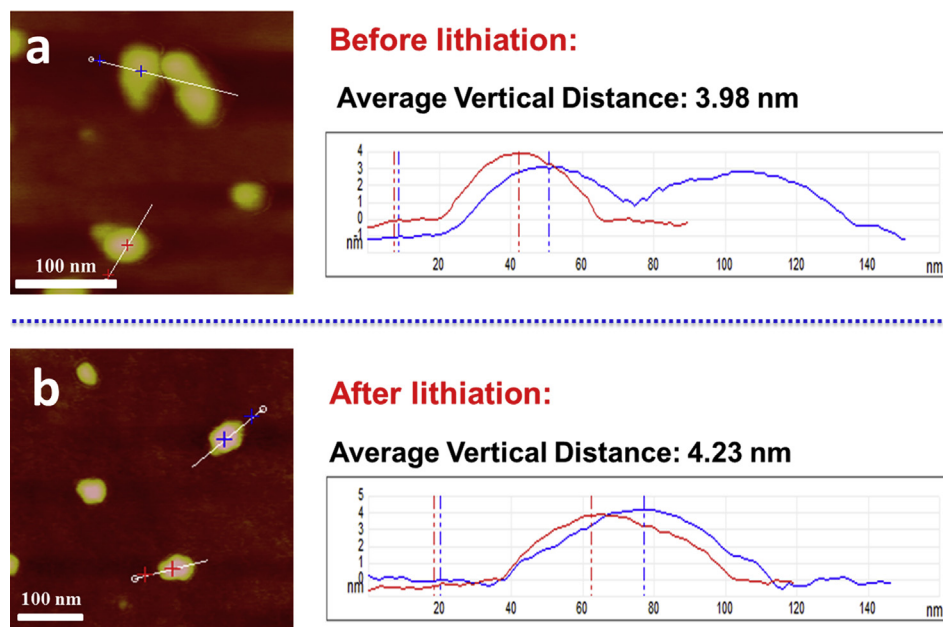


Fig. 2. The AFM images and height profiles of as-prepared (a) ultrathin non-lithiated V_6O_{13} nanosheets and (b) ultrathin lithiated V_6O_{13} nanosheets.

thickness, a 5% enlargement, reveals that the pre-lithiation process do not produce a large change for V_6O_{13} crystal structure.

3.2. Electrical transport properties

The smallest electrochemical devices based on nanosheet cathodes were assembled to reveal the intrinsic electrical conductivity changes at single nanosheet level (Fig. 3a). In the devices, as-prepared nanosheets were chosen as cathode, one flake of highly ordered pyrolytic graphite (HOPG) was chosen as anode and 1 M solution of $LiPF_6$ in ethylene carbon/dimethyl carbonate was used as the electrolyte. No conductive carbon additives or binders were brought into the systems, which can provide insights on the intrinsic electrical conductivity changes that traditional battery test strategies cannot offer. Fig. 3b shows the nanosheets cathode before and after Li^+ intercalation which shows the good contact between nanosheets and gold current collector. The electrical properties of nanosheets were *in situ* recorded during the Li^+ intercalation process. Initially, at a voltage of 500 mV, non-lithiated sample shows a current of 51 nA, while pre-lithiated V_6O_{13} nanosheets deliver a much higher current of 573 nA which shows that the conductance of ultrathin nanosheets is improved by almost one order of magnitude after pre-lithiation process (Fig. 3c and d), which may result from the increased charge carrier concentration [30,31]. It reveals the great enhancement of electrical conductivity of ultrathin V_6O_{13} nanosheets when the unique ultrathin morphology was kept. Along with Li^+ intercalation by discharge from 3.5 to 2 V, the ultrathin non-lithiated V_6O_{13} nanosheets conductance decreased over 2 orders (1 nA at 500 mV, Fig. 3c) showing a tremendous structural change when many lithium ions have intercalated into the vanadium oxide layered structure. Notably, the conductance of ultrathin pre-lithiated vanadium oxide nanosheets still remained at a high level after Li^+ intercalation (187 nA at 500 mV, Fig. 3d) indicating that the pre-lithiation process could alleviate the structural change for nanosheets cathode. It provides the direct evidence for the expectation that the pre-lithiation nanosheets may accommodate Li^+ intercalation more easily which could result in a great enhancement of cycling stability.

3.3. Electrochemical performance

Comparative electrochemical performance (Fig. 4) of ultrathin non-lithiated and lithiated V_6O_{13} nanosheet cathodes were evaluated in two-electrode coin-type cells using metallic Li as a counter and referenced electrode. The voltage profiles of fabricated samples during the first cycle at the current density of 100 mA g^{-1} between 1.5 and 4.0 V are shown in Fig. 4a. The initial discharge capacity of ultrathin V_6O_{13} nanosheets is 331 mAh g^{-1} . The typical voltage curves, presenting four main charge and discharge plateaus, show that there are four principal reactions between the electrodes. After lithiation treatment, the first charge and discharge capacities change into 328 and 301 mAh g^{-1} , respectively. It is observed that the proportions of main charge and discharge plateaus of ultrathin lithiated V_6O_{13} nanosheet cathodes differ from the non-lithiated sample.

Simultaneously, the cyclic voltammetric (CV) curves show the same results. In the first discharge cycle, four sharp peaks at $\sim 2.60 \text{ V}$, $\sim 2.40 \text{ V}$, $\sim 2.28 \text{ V}$ and $\sim 1.89 \text{ V}$, revealing the main redox reactions, are shown for ultrathin V_6O_{13} nanosheet electrode (Fig. 4b). Among them, the peak at $\sim 1.89 \text{ V}$ shares the highest proportion. In addition, these peaks in the second discharge cycle display less distinction with that of the first cycle, indicating a major structural conservation after the second charge and discharge. For ultrathin lithiated V_6O_{13} nanosheets, a new reduction peak at $\sim 2.30 \text{ V}$ is found in the first cycle (Fig. 4c), while two adjacent peaks at $\sim 2.40 \text{ V}$ and $\sim 2.28 \text{ V}$ found in non-lithiated sample are absent. Besides, the peak at $\sim 2.30 \text{ V}$ shares the highest proportion compared to the other two reduction peaks at $\sim 2.61 \text{ V}$ and $\sim 2.00 \text{ V}$. During the pre-lithiation procedure, the pre-intercalation process of Li may result in a structural pre-distortion and the occupation of different lithium sites [7,32,33]. Such a slightly pre-distorted V_6O_{13} structure may avoid the occurrence of change in phase or valence state in the initial charge and discharge process, which then enhances the peak at $\sim 2.30 \text{ V}$ consequently. Moreover, the CV curve in the second cycle shows much less distinction with that of the first cycle after lithiation, indicating a better structural maintain after Li insertion/extraction. A large increase of peak current was also noticed after lithiation, implying a

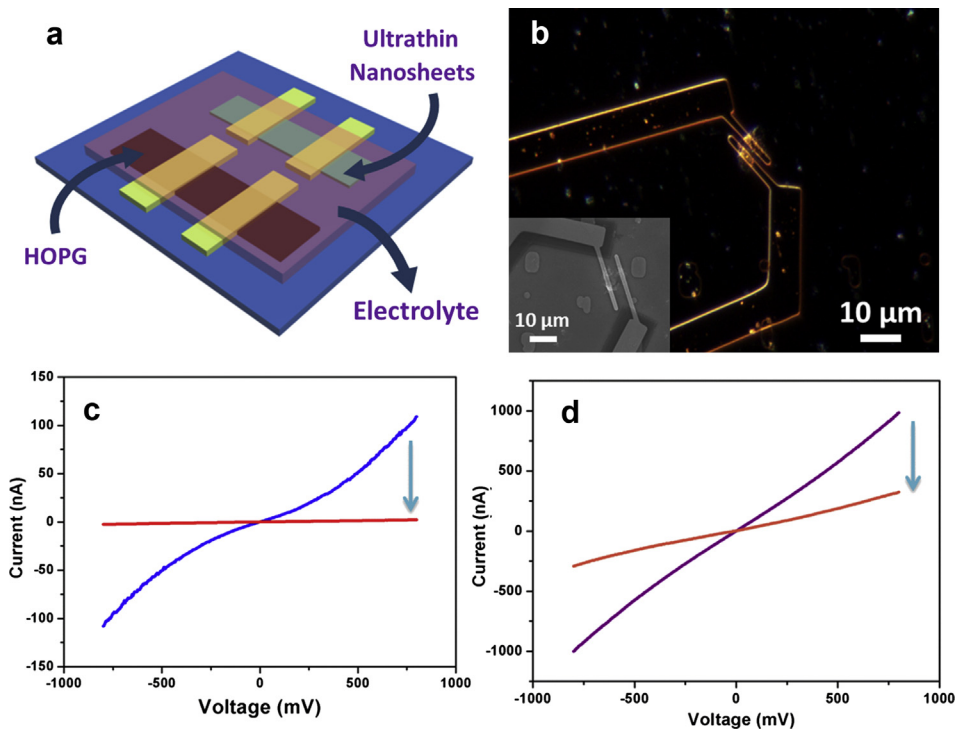


Fig. 3. (a) Schematic illustration of assembled nanosheet cathodes based energy storage device. (b) The dark-field optical microscopy image of nanosheets cathode before Li^+ intercalation. Inset shows the SEM image of nanosheets cathode after Li^+ intercalation. (c, d) The transport properties of non-lithiated (c) and pre-lithiated nanosheets cathode (d) before and after Li^+ intercalation.

great enhancement of electronic transport of as-prepared V_6O_{13} cathodes.

Fig. 4d and e displays the cycling performance comparison of the as-prepared two nanostructured samples at the current densities of 100 and 1000 mA g^{-1} , respectively. Due to the retain of the

ultrathin morphology in pre-lithiation process, the very high initial discharge capacities of 331 and 301 mAh g^{-1} measured at the current density of 100 mA g^{-1} (approximately C/3) are shown before and after lithiation, respectively. During the discharge process, the electrochemical reactions are:

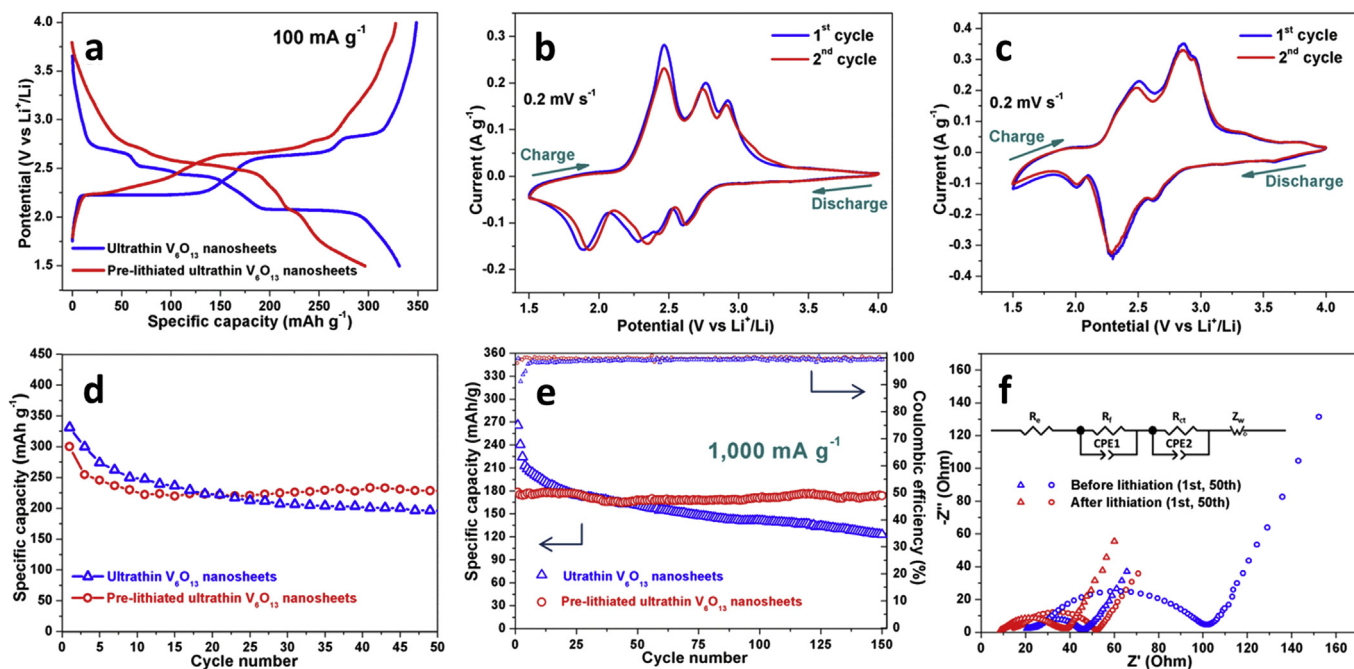
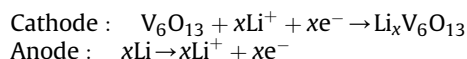


Fig. 4. (a) The first charge/discharge voltage profiles at the current density of 100 mA g^{-1} between 1.5 and 4.0 V vs. Li^+/Li of as-prepared samples; (b) cyclic voltammograms of (b) non-lithiated ultrathin V_6O_{13} nanosheets and (c) ultrathin lithiated V_6O_{13} nanosheets at a scan rate of 0.2 mV s^{-1} between 1.5 and 4.0 V vs Li^+/Li in the first and second cycles; the cycling performance of as-prepared samples at the current density of (d) 100 mA g^{-1} and (e) 1000 mA g^{-1} ; (f) AC impedance plots of the products, from 0.01 Hz to 100 kHz.



In the above redox process, x presents the inserted lithium ion amount. At the current density of 100 mA g^{-1} , approximately 6.34 mol and 5.77 mol lithium have inserted into the V_6O_{13} structure per mole before and after the pre-lithiation process, respectively. These calculations are based on the equation: $n = (3.6 M \cdot C) / F$, where n represents the inserted lithium ion amount (mol), F represents the Faraday constant (C mol^{-1}), C represents the capacity (mAh g^{-1}), M represents the molecular weight (g mol^{-1}) [34]. The discharge capacity of non-lithiated sample decreases to 196 mAh g^{-1} after 50 cycles, while the 50th discharge capacity remains 229 mAh g^{-1} after lithiation, showing a higher capacity retention of 76%. Although pre-lithiated V_6O_{13} nanosheet electrode delivers a lower specific capacity, it depicts a better cycling performance. At a much higher current density of 1000 mA g^{-1} , it is surprisingly found that ultrathin V_6O_{13} nanosheets still exhibit a desirable initial specific discharge capacity of 265 mAh g^{-1} . It demonstrates that both remarkable capacity and high rate capability are realized simultaneously. During 150 charge and discharge cycles, its specific discharge capacity decreases to 123 mAh g^{-1} gradually. After lithiation treatment, the initial specific discharge capacity is 178 mAh g^{-1} , which is much higher than the commercially used cathode materials. Its specific discharge capacity during 150th cycle maintains at 174 mAh g^{-1} with an excellent capacity retention of 98%. Higher coulombic efficiency value shown in Fig. 4e also demonstrates a better cycling performance compared with non-lithiated sample. The electrochemical impedance spectra (EIS) (Fig. 4f) were performed to further support the enhancements in electrochemical performance through pre-lithiation method. According to the simulated result for the electrochemical impedance spectra, the R_f is found but low enough to be neglected. The Nyquist plots indicate that the charge transfer resistance (R_{ct}) of ultrathin pre-lithiated V_6O_{13} nanosheet cathode is 12Ω , much lower than that of the non-lithiated sample (27Ω). Moreover, after 50 cycles measured at the current density of 1000 mA g^{-1} , the increase of R_{ct} for pre-lithiated sample is only 2Ω , much less than that of 35Ω for non-lithiated sample, indicating a desirable structural stability and cycling performance of pre-lithiated sample.

Rate performance of pre-lithiated sample at progressively increased current density was further measured, ranging from 200 to 2000 mA g^{-1} (Fig. 5a and b). Even at a higher current density of 2000 mA g^{-1} , it still delivers a discharge capacity of 150 mAh g^{-1} . Stable cycling performances were obtained for all rates. When the current density turned back to 500 mA g^{-1} , about 99.5% of the capacity is recovered, showing an excellent rate performance. The excellent rate performance is mainly attributed to the 2D layered characteristics, including their ultrathin structure and aligned channels for Li diffusion with small dimension, providing a high charge/discharge capacity and excellent rate performance [35–37]. The high specific capacities, excellent cycling performance and rate performance of ultrathin pre-lithiated V_6O_{13} nanosheets could be attributed to the rapid ionic and electronic transport. On one hand, the ultrathin structure, which shortens the diffusion paths and improves kinetics of charge carrier transport greatly, could enable lithium ions transport more quickly [22]. On the other hand, the pre-lithiation enables the structural stability and high electrical conductivity during the lithium insertion/extraction, thereby greatly enhances the cycling stability.

Compared with the previous work, as-prepared ultrathin pre-lithiated V_6O_{13} nanosheet cathodes exhibit the greatly improved reversible capacity even at a high current density of 1000 mA g^{-1} (approximately 6 C), and 2000 mA g^{-1} (approximately 14 C), which has never been reported for V_6O_{13} cathodes. Moreover, to our

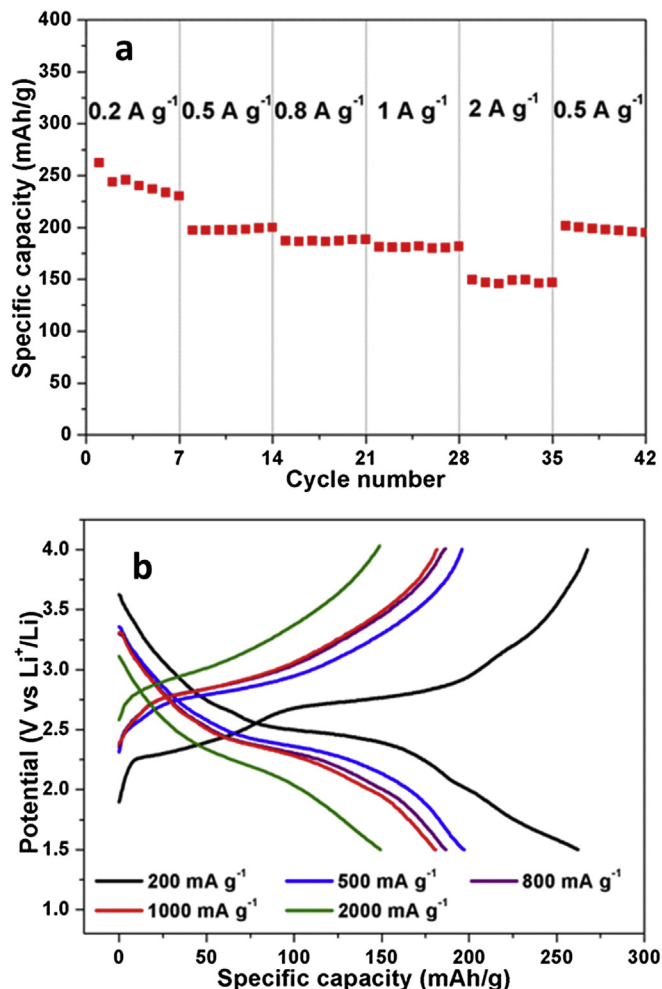


Fig. 5. (a) Rate performance and (b) initial charge–discharge curves of ultrathin lithiated V_6O_{13} nanosheets at various current densities from 200 to 2000 mA g^{-1} .

knowledge, the highest capacity retention of V_6O_{13} cathodes is achieved here [10–13]. These considerable specific capacity, fast charge/discharge process, long cycling life and ultrathin configuration indicate that the as-prepared V_6O_{13} cathodes could meet the requirements as high-capacity, high-rate, and long-life rechargeable lithium batteries.

4. Conclusion

The novel ultrathin pre-lithiated V_6O_{13} nanosheet cathodes were prepared through low-temperature exfoliation approach in argon, followed by a unique secondary hydrothermal lithiation process. The smallest electrochemical devices based on nanosheet cathodes were fabricated and ultrathin pre-lithiated V_6O_{13} nanosheets demonstrated the enhanced intrinsic advantages in electrical conductivity. Meanwhile, ultrathin pre-lithiated nanosheets exhibited the greatly improved electrochemical performance especially the cycling properties. At a current density of 100 mA g^{-1} , it delivered a reversible discharge capacity as high as 301 mAh g^{-1} . The capacity retention can reach up to 98% after 150 cycles at a current density of 1000 mA g^{-1} . Our work presented a great platform to investigate the intrinsic properties of two-dimensional nanomaterials, which is closely related to their electrochemical performance. It could also help us a better understanding of the direct reasons in different cyclability for other electrodes and

enable us to obtain long-life electrode materials. The ultrathin prelithiation V_6O_{13} nanosheet cathodes have been demonstrated to be an ideal candidate for next-generation large-scale energy storage devices.

Acknowledgments

This work was supported by the National Basic Research Program of China (2013CB934103, 2012CB933003), the National Natural Science Foundation of China (51272197 and 51072153), the International Science & Technology Cooperation Program of China (2013DFA50840), the Foundation of State Key Laboratory of Advanced Technology for Materials Synthesis and Processing (2013-ZD-7), the Fundamental Research Funds for the Central Universities (2012-yb-02), and the Students Innovation and Entrepreneurship Training Program (201311049701007). Thanks to Prof. C. M. Lieber of Harvard University and Prof. D. Y. Zhao of Fudan University for strong support and stimulating discussion. Thanks to Prof. Y. Gogotsi of Drexel University for very insightful suggestions.

Appendix A. Supplementary data

Supplementary data related to this article can be found at <http://dx.doi.org/10.1016/j.jpowsour.2014.01.017>.

References

- [1] Y. Gogotsi, P. Simon, *Science* 334 (2011) 917–918.
- [2] X. Xu, Y.Z. Luo, L.Q. Mai, Y.L. Zhao, Q.Y. An, L. Xu, F. Hu, L. Zhang, Q.J. Zhang, *NPG Asia Mater.* 4 (2012) e20.
- [3] C. Liu, F. Li, L.-P. Ma, H.-M. Cheng, *Adv. Mater.* 22 (2010) E28–E62.
- [4] S. Chu, A. Majumdar, *Nature* 488 (2012) 294–303.
- [5] (a) B. Dunn, H. Kamath, J.-M. Tarascon, *Science* 334 (2011) 928–935; (b) P.G. Bruce, B. Scrosati, J.-M. Tarascon, *Angew. Chem. Int. Ed.* 47 (2008) 2930–2946.
- [6] M.S. Whittingham, *Chem. Rev.* 104 (2004) 4271–4301.
- [7] N.A. Chernova, M. Roppolo, A.C. Dillon, M.S. Whittingham, *J. Mater. Chem.* 19 (2009) 2526–2552.
- [8] J.X. Zhu, L.J. Cao, Y.S. Wu, Y.J. Gong, Z. Liu, H.E. Hoster, Y.H. Zhang, S.T. Zhang, S.B. Yang, Q.Y. Yan, P.M. Ajayan, R. Vajtai, *Nano Lett.* 13 (2013) 5408–5413.
- [9] T. Yao, L. Liu, C. Xiao, X.D. Zhang, Q.H. Liu, S.Q. Wei, Y. Xie, *Angew. Chem. Int. Ed.* 52 (2013) 7554–7558.
- [10] W. Murphy, P.A. Christian, F.J. DiSalvo, J.N. Carides, *J. Electrochem. Soc.* 126 (1979) 497–499.
- [11] D.W. Murphy, P.A. Christian, *Science* 205 (1979) 651–656.
- [12] K. West, B. Zachau-Christiansen, T. Jacobsen, S. Atlung, *J. Power Sources* 14 (1985) 235–245.
- [13] K. West, B. Zachau-Christiansen, T. Jacobsen, *Electrochim. Acta* 28 (1983) 1829–1833.
- [14] H.Q. Li, P. He, Y.G. Wang, E. Hosono, H.S. Zhou, *J. Mater. Chem.* 21 (2011) 10999–11009.
- [15] T. Schmitt, A. Augustsson, J. Nordgren, L.-C. Duda, J. Höwing, T. Gustafsson, U. Schwingenschlögl, V. Eyert, *Appl. Phys. Lett.* 86 (2005) 064101.
- [16] D. Chen, H.B. Feng, J.H. Li, *Chem. Rev.* 112 (2012) 6027–6053.
- [17] N. Li, Z. Chen, W. Ren, F. Li, H.-M. Cheng, *Proc. Natl. Acad. Sci.* 109 (2012) 17360–17365.
- [18] J. Liu, X.-W. Liu, *Adv. Mater.* 24 (2012) 4097–4111.
- [19] Y. Du, Z. Yin, J. Zhu, X. Huang, X.-J. Wu, Z. Zeng, Q. Yan, H. Zhang, *Nat. Commun.* 3 (2012) 1177.
- [20] H. Hwang, H. Kim, J. Cho, *Nano Lett.* 11 (2011) 4826–4830.
- [21] J. Feng, X. Sun, C. Wu, L. Peng, C. Lin, S. Hu, J. Yang, Y. Xie, *J. Am. Chem. Soc.* 133 (2011) 17832–17838.
- [22] C. Xu, Y. Zeng, X.H. Rui, N. Xiao, J.X. Zhu, W.Y. Zhang, J. Chen, W.L. Liu, H.T. Tan, H.H. Hng, Q.Y. Yan, *ACS Nano* 6 (2012) 4713–4721.
- [23] (a) A.Q. Pan, H.B. Wu, L. Yu, X.W. Lou, *Angew. Chem. Int. Ed.* 52 (2013) 2226–2230; (b) D.D. Vaughn, O.D. Hentz, S. Chen, D. Wang, R.E. Schaak, *Chem. Commun.* 48 (2012) 5608–5610.
- [24] H.Y. Wang, S.Q. Liu, Y. Ren, W.J. Wang, A.D. Tang, *Energy Environ. Sci.* 5 (2012) 6173–6179.
- [25] M. Naguib, J. Halim, J. Lu, K.M. Cook, L. Hultman, Y. Gogotsi, M.W. Barsoum, *J. Am. Chem. Soc.* 135 (2013) 15966–15969.
- [26] C.Z. Wu, X.L. Lu, L.L. Peng, K. Xu, X. Peng, J.L. Huang, G.H. Yu, Y. Xie, *Nat. Commun.* 4 (2013) 2431.
- [27] M.R. Lukatskaya, O. Mashtalir, C.E. Ren, Y. Dall’Agnese, P. Rozier, P.L. Taberna, M. Naguib, P. Simon, M.W. Barsoum, Y. Gogotsi, *Science* 341 (2013) 1502–1505.
- [28] H.Y. Wang, Y. Ren, Y. Wang, W.J. Wang, S.Q. Liu, *CrystEngComm* 14 (2012) 2831–2836.
- [29] L.Q. Mai, Y.J. Dong, L. Xu, C.H. Han, *Nano Lett.* 10 (2010) 4273–4278.
- [30] L.Q. Mai, B. Hu, W. Chen, Y. Qi, C. Lao, R. Yang, Y. Dai, Z.L. Wang, *Adv. Mater.* 19 (2007) 3712–3716.
- [31] D.K. Chakrabarty, D. Guha, A.B. Biswas, *J. Mater. Sci.* 11 (1976) 1347–1353.
- [32] (a) Y. Mizuno, E. Hosono, T. Saito, M. Okubo, D. Nishio-Hamane, K. Oh-ishi, T. Kudo, H.S. Zhou, *J. Phys. Chem. C* 116 (2012) 10774–10780; (b) S. Luo, K. Wang, J.P. Wang, K. Jiang, Q.Q. Li, S.S. Fan, *Adv. Mater.* 24 (2012) 2294–2298.
- [33] R. Malik, D. Burch, M. Bazant, G. Ceder, *Nano Lett.* 10 (2010) 4123–4127.
- [34] J. Desilvestro, O. Haas, *J. Electrochem. Soc.* 137 (1990) 5C–22C.
- [35] X.H. Rui, X.X. Zhao, Z.Y. Lu, H.T. Tan, D.H. Sim, H.H. Hng, R. Yazami, T.M. Lim, Q.Y. Yan, *ACS Nano* 7 (2013) 5637–5646.
- [36] J.W. Seo, J.T. Jang, S.W. Park, C. Kim, B. Park, J. Cheon, *Adv. Mater.* 20 (2008) 4269–4273.
- [37] S.B. Yang, X.L. Feng, L.J. Zhi, Q. Cao, J. Maier, *Adv. Mater.* 22 (2010) 838–842.